ELSEVIER

Journal of Power Sources 89 (2000) 93–101

JOURNAL OF POWER SOURCES

www.elsevier.com/locate/jpowsour

Fast-charging of a lead–acid cell: effect of rest period and depolarization pulse

Sung Chul Kim, Won Hi Hong *

Department of Chemical Engineering, Korea Advanced Institute of Science, and Technology, 373-1 Kusung-dong, Yusung-gu, Taejeon 305-701, South Korea

Received 10 December 1999; accepted 31 December 1999

Abstract

Cell behavior is numerically investigated for fast charging of a lead–acid cell under constant current or pulsed current. A model used in the simulation has been developed to predict the cell performance by considering the solid-state reaction at the negative electrode. By incorporating a rest period and a depolarization pulse on high rate charge, it is possible to avoid deterioration of the cell performance due to an increase in internal resistance. Thus, fast charging of a lead–acid cell can be achieved without a loss of cycle-life, despite the fact that higher currents are forced into the cell.

Keywords: Lead–acid cell; Fast charge; Electrode kinetics; Mathematical modeling

1. Introduction

The fast charging of a lead–acid battery, or indeed other secondary rechargeable batteries, is a key technology for electric vehicles. Considerable researches have been performed to reduce the time required to fully charge a battery without loss of capacity or life. To charge at high efficiency and for good cycle-life, it is important that the internal resistance of the cell must be kept low.

Gu et al. [1] examined the voltage behaviour and the variation of electrolyte concentration for constant-current charge at 25°C and −18°C. Maja et al. [2] investigated simulation of the discharge and charge processes by studying the effect of various parameters such as plate dimensions, amount of acid, and porosity of the active material. They also observed cell voltage as a function of the charging current intensity and the charging modality, e.g., single or stepped. The battery was charged up to 70% of the nominal capacity, and then recharged after a rest period.

Calasanzio et al. [3] simulated not only constant-current charge, for which the porosity of the active material was found to influence the charge returned, but also step charging with and without rest periods. Chang et al. [4] examined the temperature rise in a flooded hybrid battery during charge. These authors found that in the first part of a rapid charge to about 40% return, resistive heating was the major contributor to the initial rise in temperature. With further charging, heat from polarization becomes more important. Gu et al. [5] investigated the discharge and charge processes by considering not only electrochemical kinetics and mass transport, but also free convection due to acid stratification.

Lam et al. [6] compared a pulsed-current technique with a constant-current recharge for the rapid charging of lead–acid cells. They examined the electrochemical characteristics and cycle-life performance with each charging method. Podrazhansky and Popp [7] used a depolarization pulse to reduce the increase in the internal resistance due to severe concentration polarization. The depolarization pulse also moderated the temperature rise of the cell. Catherino et al. [8] represented the charging curves at constant current over a range of temperature by combining the individual effects of battery charging and gassing. Kim and Hong [9] observed the effect of the electrode parameters, such as the charge-reaction concentration exponent, morphology parameters and limiting current density on charge performance.

In this work, a simulation is made of the effects of rest period and a depolarization pulse on the charge behaviour

* Corresponding author.
E-mail address: whhong@hanbit.kaist.ac.kr (W.H. Hong).

0378-7753/00/$ - see front matter
PII: S0378-7753(00)00381-5

Table 1
Governing equations for each region

	Positive electrode	Reservoir	Separator	Negative electrode
Porosity variation	$(\partial\varepsilon/\partial t) = [1/(2F)]a_1 j$	$\varepsilon = 1$	$\varepsilon = \varepsilon_{\text{sep}}$	$(\partial\varepsilon/\partial t) = [1/(2\text{F})]a_1 j$
Ohm's law in solid	$i_1 = \sigma^{*}\nabla\phi_1$	$i_1 = 0$	$i_1 = 0$	$i_1 = \sigma^{*}\nabla\phi_1$
Ohm's law in liquid	$i_2 = -\kappa^{*}\nabla\phi_2 - \kappa^{**}\nabla(\ln c)$	$i_2 = -\kappa^{*}\nabla\phi_2 - \kappa^{**}\nabla(\ln c)$	$i_2 = -\kappa^{*}\nabla\phi_2 - \kappa^{**}\nabla(\ln c)$	$i_2 = -\kappa^{*}\nabla\phi_2 - \kappa^{**}\nabla(\ln c)$
Mass balance of electrolyte	$[\partial(\varepsilon c)/\partial t] + v^{*}\cdot\nabla c = \nabla\cdot(D^{*}\nabla c) + [(a_2 j)/(2F)]$	$[\partial(\varepsilon c)/\partial t] + v^{*}\cdot\nabla c = \nabla\cdot(D^{*}\nabla c) + [(a_2 j)/(2F)]$	$[\partial(\varepsilon c)/\partial t] + v^{*}\cdot\nabla c = \nabla\cdot(D^{*}\nabla c) + [(a_2 j)/(2F)]$	$[\partial(\varepsilon c)/\partial t] + v^{*}\cdot\nabla c = \nabla\cdot(D^{*}\nabla c) + [(a_2 j)/(2F)]$
Electrode kinetics (charge)	$j = ai_{\text{o1,ref}}\left(1 - \frac{Q}{Q_{\max}}\right)\left(\frac{c}{c_{\text{ref}}}\right)^{\gamma 1} \times \left[\exp\left(\alpha_{\text{a1}}\frac{F\eta}{RT}\right) - \exp\left(\alpha_{\text{c1}}\frac{F\eta}{RT}\right)\right]$	$\phi_1 = 0$	$\phi_1 = 0$	$j = ai_{\text{o7,ref}}\left(1 - \frac{Q}{Q_{\max}}\right)\left(\frac{c}{c_{\text{ref}}}\right)^{\gamma 4} \times \frac{1 - \exp\left[(\alpha_{\text{a4}} + \alpha_{\text{c4}})\frac{F\eta}{RT}\right]}{\frac{ai_{\text{o4,ref}}}{j_{\text{lim}}} - \exp\left[\alpha_{\text{c4}}\frac{F\eta}{RT}\right]}$
(Depolarization)	$j = ai_{\text{o1,ref}}\left(\frac{c}{c_{\text{ref}}}\right)^{\gamma 1} \times \left[\exp\left(\alpha_{\text{a1}}\frac{F\eta}{RT}\right) - \exp\left(\alpha_{\text{c1}}\frac{F\eta}{RT}\right)\right]$			$j = ai_{\text{o4,ref}}\left(\frac{c}{c_{\text{ref}}}\right)^{\gamma 4} \times \frac{1 - \exp\left[(\alpha_{\text{a4}} + \alpha_{\text{c4}})\frac{F\eta}{RT}\right]}{\frac{ai_{\text{o4,ref}}}{j_{\text{lim}}} - \exp\left[\alpha_{\text{c4}}\frac{F\eta}{RT}\right]}$

Table 2
Boundary conditions for each region

Centers of positive and negative electrode	Interface between positive electrode and reservoir	Interface between reservoir and separator	Interface between separator and negative electrode
$\nabla c = 0$	$\varepsilon^* \nabla c\|_+ = \nabla c\|_{res}$	$D \cdot \nabla c - c v^*\|_{res} = D^* \cdot \nabla c - c v^*\|_{sep}$	$\varepsilon^* \nabla c\|_{sep} = \varepsilon^* \nabla c\|_-$
$\nabla \varepsilon$	$\varepsilon^* \nabla \phi_2\|_+ = \nabla \phi_2\|_{res}$	$\varepsilon = \varepsilon_{sep}$	$\varepsilon^* \nabla \phi_2\|_{sep} = \varepsilon^* \nabla \phi_2\|_-$
$\nabla \phi_2 = 0$	$(\partial \varepsilon / \partial t) = [1/(2F)] a_1 j$	$i_2 = i$	$(\partial \varepsilon / \partial t) = [1/(2F)] a_1 j$
$i_2 = 0$	$i_2 = i$	$\phi_1 = 0$	$i_2 = i$
$\phi_1 = 0$ (positive electrode)			
$j = a i_{o4,ref} \left(1 - \frac{Q}{Q_{max}}\right) \left(\frac{c}{c_{ref}}\right)^{\gamma 4} \times \frac{1 - \exp\left[(\alpha_{a4} + \alpha_{c4}) \frac{F\eta}{RT}\right]}{\frac{a i_{o4,ref}}{j_{lim}} - \exp\left[\alpha_{c4} \frac{F\eta}{RT}\right]}$			
(Negative electrode for charge)	$\nabla \phi_1 = 0$	$\nabla \phi_2 - [(RT)/F](1 - 2t_+^o) \nabla(\ln c)\|_{res} = \varepsilon^* [\nabla \phi_2 - [(RT)/F](1 - 2t_+^o) \nabla(\ln c)]\|_{sep}$	$\nabla \phi_1 = 0$
$j = a i_{o4,ref} \left(\frac{c}{c_{ref}}\right)^{\gamma 4} \times \frac{1 - \exp\left[(\alpha_{a4} + \alpha_{c4}) \frac{F\eta}{RT}\right]}{\frac{a i_{o4,ref}}{j_{lim}} - \exp\left[\alpha_{c4} \frac{F\eta}{RT}\right]}$			
(Negative electrode for depolarization)			

of a lead–acid cell, using a mathematical model, which have been developed during the studies of cell performance, both during constant-current charge [9] and during discharge [10,11]. The results of the simulation will help to determine the best charging method, which will reduce the time to full charge and will not cause damage to the battery.

2. Theoretical background

The governing equations used to describe the porous electrode are material balance of a transport species, ohmic loss in liquid and solid phases, and conservation of charge. In a macroscopic treatment, the actual pore geometry is disregarded. If the potentials in the solid and the liquid phase are defined, these quantities are assumed to be continuous functions of time and space coordinates. In effect, the electrode is treated as the superposition of two continua: one represents the solution, the other represents the matrix [12].

The electrode reactions during the charging of a lead–acid cell are as follows.

Positive electrode:

$$PbSO_4(s) + 2H_2O \rightarrow PbO_2(s) + HSO_4^- + 3H^+ + 2e^-. \quad (1)$$

Negative electrode:

$$PbSO_4(s) + 2e^- + H^+ \rightarrow Pb(s) + HSO_4^-. \quad (2)$$

Lead sulfate is converted into lead dioxide (positive electrode) and lead (negative electrode) during charge.

Note that the electrochemical reaction can only take place where electrons can be supplied or removed, which means that this conversion is not possible on the surface of the lead sulfate, as lead sulfate does not conduct electric current. For this reason, the Pb^{2+} ions should be dissolved

Table 3
Coefficients and effective properties used in model equations

	Positive electrode	Reservoir	Separator	Negative electrode
a_1	$\frac{MW_{PbSO_4}}{\rho_{PbSO_4}} - \frac{MW_{PbO_2}}{\rho_{PbO_2}}$	–	–	$\frac{MW_{Pb}}{\rho_{Pb}} - \frac{MW_{PbSO_4}}{\rho_{PbSO_4}}$
a_2	$3 - 2t_+^o$	0	0	$1 - 2t_+^o$
σ^*	$\sigma_{PbO_2} \varepsilon^{exm1}$	–	–	$\sigma_{Pb} \varepsilon^{exm4}$
κ^*	$\kappa \varepsilon^{ex1}$	κ	$\kappa \varepsilon_{sep}^{ex3}$	$\kappa \varepsilon^{ex4}$
κ^{**}	$[(RT)/F] \kappa \varepsilon^{ex1} (2t_+^o - 1)$	$[(RT)/F] \kappa (2t_+^o - 1)$	$[(RT)/F] \kappa \varepsilon_{sep}^{ex3} (2t_+^o - 1)$	$[(RT)/F] \kappa \varepsilon^{ex4} (2t_+^o - 1)$
D^*	$D \varepsilon^{ex1}$	D	$D \varepsilon_{sep}^{ex3}$	$D \varepsilon^{ex4}$

and transported by diffusion to the conductive electrode surface [13].

The kinetics of a porous electrode are affected by the local activity, overpotential, electrolyte concentration, and current density as a function of electrode structure. For a dissolution–precipitation mechanism, it is assumed that the electrode reactions in the negative electrode consist of three steps, i.e., dissolution of lead sulfate, diffusion of lead ions to the active sites, and precipitation of lead [14]. Thus, the electrode reaction rate at the negative electrode, including the solid-state reaction rate and the effect of electrolyte concentration, is expressed as a transfer-current density [12]. The transfer-current density at the positive electrode can be obtained from the Butler–Volmer equation.

Since a material balance on the solid phase shows how the porosity changes with the extent of reaction, the variation of the electrode porosity at each location can be equated to the density differences between the solid products and reactants that result from the local transfer current [12].

With the assumption of uniformity and homogeneity of the electrode in other directions, the differential material balance of a dissolved species for a one-dimensional system can be expressed. Diffusivity and conductivity used here are related to both the porosity and tortuosity of the electrode.

The mass transfer in the electrolyte solution is given by convection, diffusion and migration of mobile ionic species. The transference number and the partial molar volume of

Table 4
Parameters used in the calculations

Parameter	Value
Positive electrode	
Half thickness of plate	0.0875 cm
Maximum charge state	2620 C cm^{-3}
Reaction parameter ($a_{max1} i_{o1,ref}$)	0.073 A cm^{-3}
α_{a1}	1.15
α_{c1}	0.85
$\gamma 1$	0.01 (charge)
$\zeta 1$	1.0
Lead dioxide conductivity	500 S cm^{-1}
ex1	1.5
exm1	0.5
Negative electrode	
Half thickness of plate	0.07 cm
Maximum charge state	3120 C cm^{-3}
Reaction parameter ($a_{max4} i_{o4,ref}$)	0.11 A cm^{-3}
α_{a4}	1.55
α_{c4}	0.45
$\gamma 4$	0.01
$\zeta 4$	1.0
Lead conductivity	4.8×10^4 S cm^{-1}
ex4	1.5
exm4	0.5
j_{lim}	-10^2 A cm^{-3} (charge) -10^5 A cm^{-3} (depolarization)
Reservoir	
Thickness of reservoir	0.07 cm
Separator	
Thickness of separator	0.022 cm
Porosity	0.60
ex3	1.50
Electrolyte	
Acid concentration	4.9×10^{-3} mol cm^{-3}
Transference number	0.72
Partial molar volume of acid	45 mol cm^{-3}
Diffusion coefficient	$D = \exp\left(\frac{2174.0}{298.15} - \frac{2174.0}{T}\right) \times (1.75 + 260.0c) \times 10^{-5}$
Conductivity	$\kappa = c \times \exp\left[1.1104 + (199.475 - 16097.781c)c + \frac{3916.95 - 99406.0c - \frac{721860}{T}}{T}\right]$

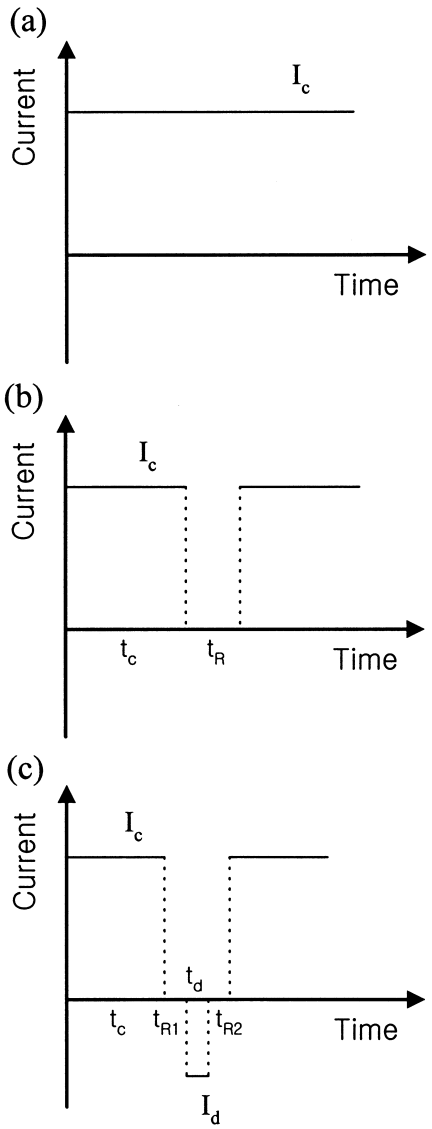

Fig. 1. Charging modalities: (a) constant current; (b) pulse current without depolarization current; (c) pulse current with depolarization current.

the electrolyte are assumed to be constant. The movement of electrons on the solid phase is followed by Ohm's law. The thickness of the electric double layer is smaller than the pore volume, so it is assumed to be electrically neutral for the electrolyte solution [15]. The divergence of total current density, therefore, is zero. All the charge leaving the solid phase enters the solution phase.

The polarization equation is used to describe the voltage jump at the interface between the solid and liquid phase and the dependence of the electrolyte concentration on the local reaction rate. In the reservoir and the separator, the transfer-current density is set at zero. The governing equations used in the numerical simulation are summarized in Table 1 [9–11].

The initial values for electrolyte concentration and porosity are obtained from the results of a discharged cell before the start of the charging process. The initial potential distribution is calculated from the kinetic equation of electrode reaction.

At the current-collectors, as the battery cell is a closed system, the potential and the electrolyte concentration are set to constant values [5]. The set of boundary conditions is given for the molar flux of the mobile ionic species, charge conservation, and porosity change. The boundary conditions used to solve the governing equations are summarized in Table 2, and the coefficients used in the development of the model are presented in Table 3.

The equations given in Tables 1 and 2 are solved by numerical methods. The space derivatives are discretized into the method of finite differences by means of three-point approximations, and the time derivatives are formulated by the Crank–Nicolson method. The set of non-linear equations in the multi-region system is solved by the iterative Newton method and modified Newman's MBAND [16]. The material properties and the cell parameters used in simulation are presented in Table 4 [9].

3. Results and discussion

The model used in the simulation includes the dissolution–precipitation mechanism in the reaction kinetics of the negative electrode. The cell used in the simulation was numerically discharged with 1.7 mA cm^{-2} for 8 h at 25°C, and then experienced rest period for 1 h at the same temperature.

The three charging methods used in the study are illustrated in Fig. 1. Fig. 1a shows that the cell is charged with a constant current to the voltage cut-off. The schedule in Fig. 1b is for pulsed-current charging; current I_c is forced into the cell for time t_c and then a rest period is

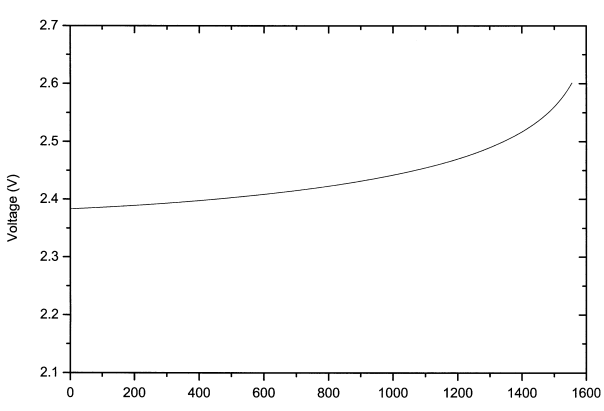

Fig. 2. Predicted voltage behaviour for constant-current charge at 30 mA cm^{-2}.

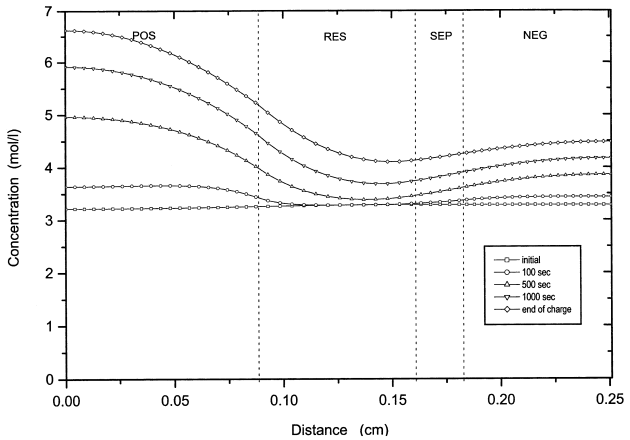

Fig. 3. Predicted profiles of acid concentration for constant current at 30 mA cm^{-2}.

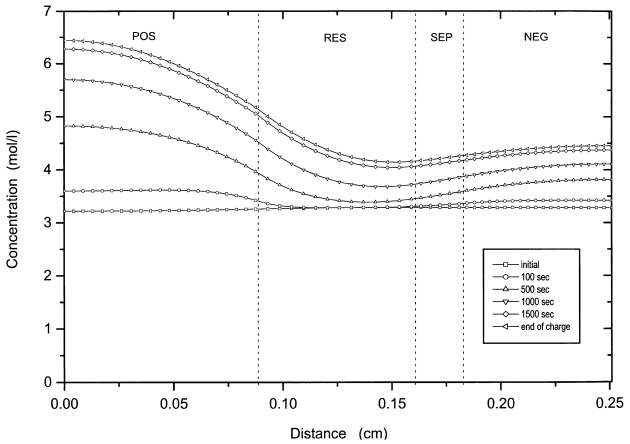

Fig. 5. Predicted profiles of acid concentration. Charging current is 30 mA cm^{-2}; duration of charge pulse is 27 s; rest period is 3 s.

followed for time t_R. A series of charging pulses and rest periods are repeated until the cell voltage reaches the voltage cut-off. The rest period has a role in relaxing the concentration gradient or polarization in the cell, which reduces the temperature rise of the cell. Fig. 1c illustrates that a depolarization current I_d is used for time t_d at the end of the rest period. Pulsed-current charging with no depolarization pulse requires a longer time to eliminate the concentration gradient. Because a rest period of short duration has little effect on the reduction of the concentration polarization, a depolarization pulse is used to decrease the concentration gradient.

The variation of cell voltage with time for charging at a constant current of 30 mA cm^{-2} to 2.6 V is shown in Fig. 2. The slope of the voltage increment increases with progressing charge, and at the end of charging, its value rises rapidly. This is because the internal resistance of the cell becomes large. Charge-acceptance or charge-current efficiency describes the share of the current, which is actually accepted by the battery and can be retrieved by subsequent discharging [13]. This value is not constant, but depends largely on the state of charge, i.e., charge-acceptance decreases with progress of the charge reaction. To ensure that the charge-acceptance has a large value, a higher surface area for the electrode and a lower internal resistance of the cell is required.

The concentration distribution for constant-current charge under the same conditions as in Fig. 2 is displaced in Fig. 3. At the start of charge, the electrolyte is uniformly distributed in the cell, but the electrolyte concentration in the positive and negative electrode increases much faster than that in other regions. Thus, for a constant-current charge, the concentration distribution is not uniform, especially at the interface between the positive electrode and the reservoir, as well as at between the negative electrode and the separator. In these two regions, the concentration gradients become steeper.

In order to charge a battery quickly, a higher current must be forced into it. One of the methods that increases the charge-acceptance and reduces the internal resistance is

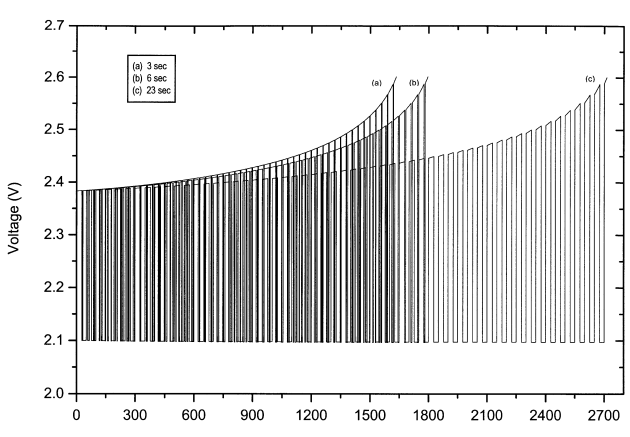

Fig. 4. Effect on rest period on cell voltage. Charging current is 30 mA cm^{-2}.

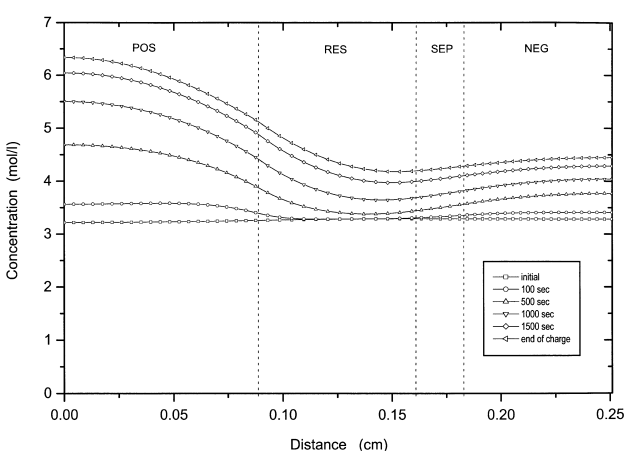

Fig. 6. Predicted profiles of acid concentration. Charging current is 30 mA cm^{-2}; duration of charge pulse is 27 s; rest period is 6 s.

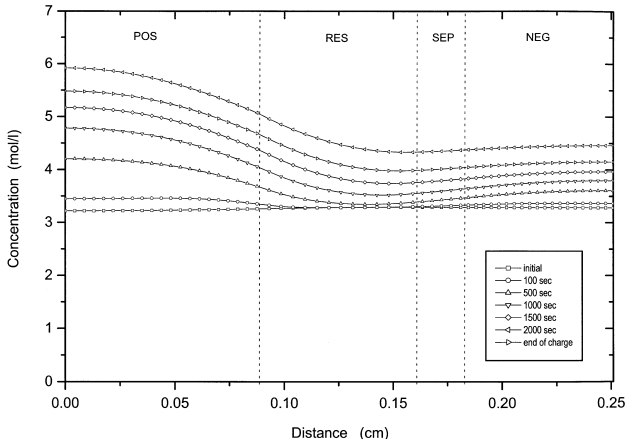

Fig. 7. Predicted profiles of acid concentration. Charging current is 30 mA cm^{-2}; duration of charge pulse is 27 s; rest period is 23 s.

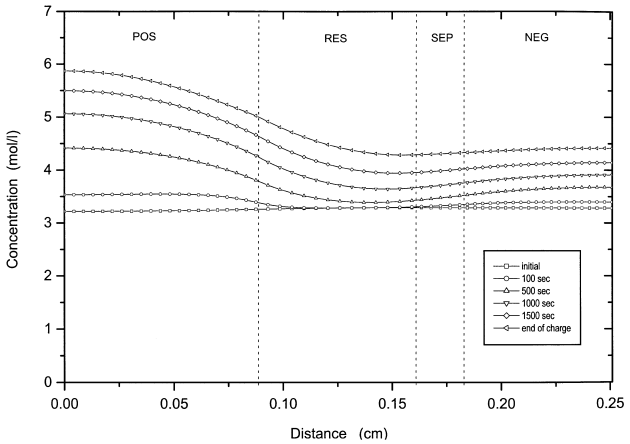

Fig. 9. Predicted profiles of acid concentration. Charging current is 30 mA cm^{-2} and duration of charge pulse is 27 s. Rest period is 3 s and duration of depolarization pulse is 2 s; depolarization current is -30 mA cm^{-2}.

pulsed-current charge. A high current is passed to the battery, which is followed by a rest period to disperse ions throughout the electrolyte. The effect of the rest period on the cell voltage with time is given in Fig. 4 for pulses of constant magnitude. The time is fixed, at 27 s and the relaxation time is 3 and 6 s, and for the changing pulse 23 s. In effect, the slope of the voltage increment is lower with a rest period and the value decreases with increasing duration of the rest period.

The concentration distributions for pulsed-current charge with the same conditions as those used in Fig. 4 are given in Figs. 5–7. For a rest period of 3 s (Fig. 5), the concentration polarization throughout the electrolyte is reduced by more than that without a rest period (cf. Fig. 2). When the duration of rest period is 6 s (Fig. 6), the concentration gradient between the negative electrode and the separator is lower than that in Fig. 5, but that between the positive electrode and the reservoir is still large. For a rest period of 23 s (Fig. 7), the behaviour of the concentration distribution is similar to that shown in Fig. 6 for a 6-s rest period.

The effect of a depolarization pulse on the charging voltage is presented in Fig. 8. During charging, positive ions move to the negative electrode and negative ions move to the positive electrode. The ions arriving at the electrode progressively shield the electrode from further charge-transfer. For a pulsed-current charge without a depolarization pulse, the rest period reduces the concentration gradient. As the duration of the rest period is increased, however, it takes more time to achieve full charge. Thus, a depolarization current serves to eliminate the concentration polarization and to reduce the charging time. Note that the duration of depolarization pulse is smaller than that of charging pulse. Therefore, the depolarization pulse should not cause any significant discharge of the battery. The duration between the charging and depolariza-

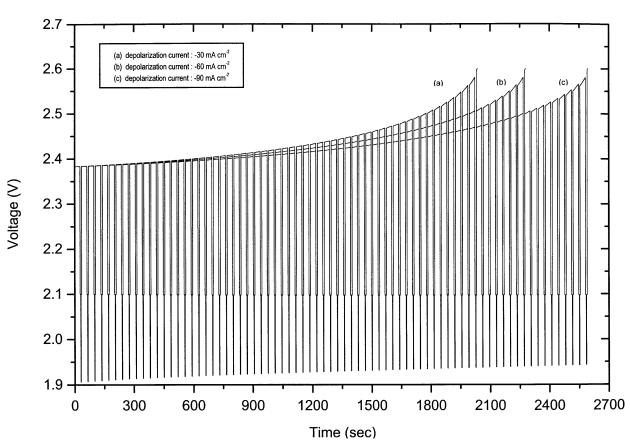

Fig. 8. Effect of depolarization pulse on charge behaviour. Charge current is 30 mA cm^{-2} and duration is 27 s. Rest period is 3 s and duration of depolarization pulse is 2 s.

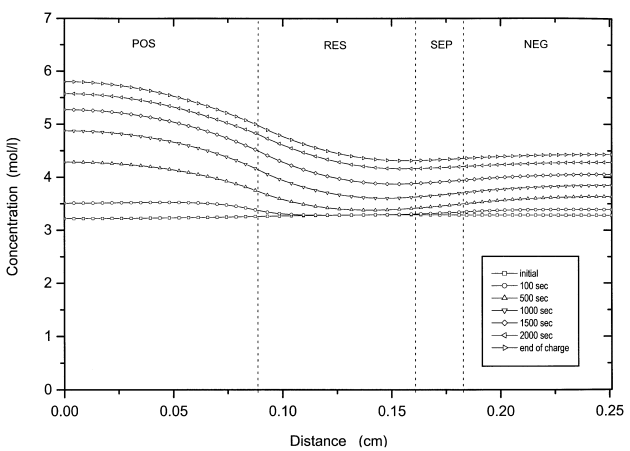

Fig. 10. Predicted profiles of acid concentration. Charging current is 30 mA cm^{-2} and duration of charge pulse is 27 s. Rest period is 3 s and duration of depolarization pulse is 2 s; depolarization current is -60 mA cm^{-2}.

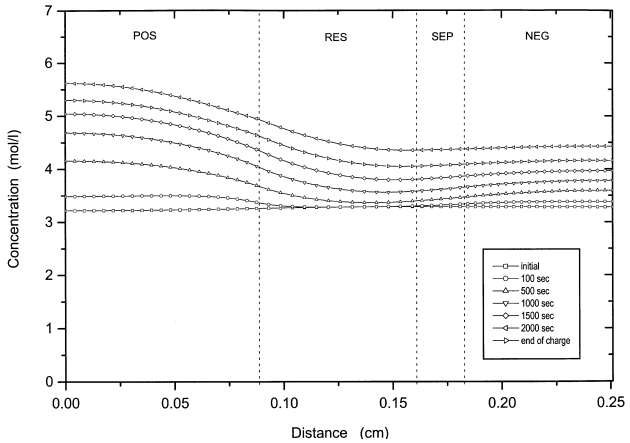

Fig. 11. Predicted profiles of acid concentration. Charging current is 30 mA cm^{-2} and duration of charge pulse is 27 s. Rest period is 3 s and duration of depolarization pulse is 2 s; depolarization current is -90 mA cm^{-2}.

tion pulse (t_R, Fig. 1c) is set to 3 s and the charging pulse is applied at 30 mA cm^{-2} for 27 s. Whereas the depolarization pulse is forced to the cell for 2 s, the current density is changed to -30, -60 and -90 mA cm^{-2}. As the current density of the depolarization pulse is increased, the voltage increment is decreased. This is because the internal resistance of the cell is reduced.

The concentration distributions for pulsed-current charge with a depolarization pulse under the same conditions as in Fig. 8 are presented in Figs. 9–11. In Fig. 9, the depolarization pulse is set at -30 mA cm^{-2} and gives similar results to those obtained with a rest period of long duration, as shown in Figs. 4 and 5. When the intensity of the depolarization pulse is -60 mA cm^{-2} (Fig. 10), the concentration gradient is reduced more than that in Fig. 9. The concentration polarization is relaxed even further at -90 mA cm^{-2}, as shown in Fig. 11. Using the depolarization pulse, it can be seen that the internal resistance is reduced and the charge-acceptance is increased.

4. Conclusions

Variations in cell voltage and concentration distribution in a lead–acid cell under constant or pulsed-current charge have been investigated using a mathematical model, which includes the dissolution–precipitation mechanism in the negative electrode. The results of applying the model can be summarized as follows.

(i) For a constant-current charge, the internal resistance of the cell has a greater effect on the charge performance. The cell voltage rises rapidly at the end of charging.

(ii) The slope of the voltage increment is lower when a rest period is included. Its value decreases with increasing duration of the rest period.

(iii) Using a pulsed current with a depolarization pulse, the internal resistance is reduced and the charge-acceptance is increased. Therefore, a high-rate charge can be performed without an increase in internal resistance or reduction in charge-acceptance.

5. List of symbols

a	active surface area of electrode (cm^2 cm^{-3})
a_1, a_2	coefficients used in governing equations and boundary conditions
a_{max}	maximum specific active surface area of electrode (cm^2 cm^{-3})
c	concentration of binary electrolyte (mol cm^{-3})
c_{ref}	reference concentration of binary electrolyte (mol cm^{-3})
D	diffusion coefficient of binary electrolyte (cm^2 s^{-1})
F	Faraday's constant (96,487 C mol^{-1})
i	total applied current density based on projected electrode area (A cm^{-2})
i_1	current density in solid phase (A cm^{-2})
i_2	current density in conducting liquid phase (A cm^{-2})
$i_{o1,ref}$	exchange current density at c_{ref} for positive electrode (A cm^{-2})
$i_{o4,ref}$	exchange current density at c_{ref} for negative electrode (A cm^{-2})
j	reaction current per unit volume of electrode (A cm^{-3})
j_{lim}	limiting current density for negative electrode (A cm^{-3})
MW_i	molecular weight of species i (g mol^{-1})
Q	charge density in electrode (C cm^{-3})
Q_{max}	theoretical maximum capacity (C cm^{-3})
R	universal gas constant (8.3143 J mol^{-1} K^{-1})
t	time (s)
t_+^o	transference number of H^+ with respect to solvent velocity
T	absolute temperature (K)
U_{PbO_2}	equilibrium potential at c_{ref} for positive electrode (V)
v^*	volume–average velocity (cm s^{-1})
x	distance from the center of positive electrode (cm)
Greek letters	
α_{a1}	anodic transfer coefficient for positive electrode
α_{c1}	cathodic transfer coefficient for positive electrode
α_{a4}	anodic transfer coefficient for negative electrode
α_{c4}	cathodic transfer coefficient for negative electrode
$\gamma 1$	concentration exponent for positive electrode
$\gamma 4$	concentration exponent for negative electrode
ε	porosity

ε_{sep}	porosity of separator
$\varepsilon_{PbO_2,ini}$	porosity of positive electrode at initial state of charge reaction
$\varepsilon_{Pb,ini}$	porosity of negative electrode at initial state of charge reaction
$\zeta 1$	morphology parameter for positive electrode
$\zeta 4$	morphology parameter for negative electrode
η	total local overpotential with respect to equilibrium potential
κ	electrolyte conductivity (S cm^{-1})
ρ_i	density of species i (g cm^{-3})
σ_i	conductivity of electrode matrix (S cm^{-1})
ϕ_1	potential in electrode matrix (V)
ϕ_2	potential in solution (V)*Superscripts*
ex	exponent on porosity
exm	empirically determined constant for tortuosity of the solid matrix

Acknowledgements

The authors acknowledge the support of Korea Storage Battery, Ltd.

References

[1] H. Gu, T.V. Nguyen, R.E. White, J. Electrochem. Soc. 134 (1987) 2953.
[2] M. Maja, G. Morello, P. Spinelli, J. Power Sources 40 (1992) 81.
[3] D. Calasanzio, M. Maja, P. Spinelli, J. Power Sources 46 (1993) 375.
[4] T.G. Chang, E.M. Valeriote, D.M. Jochim, J. Power Sources 48 (1994) 163.
[5] W.B. Gu, C.Y. Wang, B.Y. Liaw, J. Electrochem. Soc. 144 (1997) 2053.
[6] L.T Lam, H. Ozgun, O.V. Lim, J.A. Hamilton, L.H. Vu, D.G. Vella, D.A.J. Rand, J. Power Sources 53 (1995) 215.
[7] Y. Podrazhansky, P.W. Popp, US Patent 5 307 000, Apr. 26 (1994).
[8] H.A. Catherino, J.F. Burgel, A. Rusek, F. Feres, J. Power Sources 80 (1999) 17.
[9] S.C. Kim, W.H. Hong, J. Power Sources, in press.
[10] S.C. Kim, W.H. Hong, J. Power Sources 77 (1999) 74.
[11] S.C. Kim, W.H. Hong, Hwahak Konghak 37 (1999) 336.
[12] J. Newman, W. Tiedemann, AIChE J. 21 (1975) 25.
[13] D. Berndt, in: Maintenance-Free Batteries, 2nd edn., Research Studies Press, Taunton, Somerset, England, 1997.
[14] P. Ekdunge, K.V. Rybalka, D. Simonsson, Electrochim. Acta 32 (1987) 659.
[15] J.S. Newman, Electrochemical Systems, 2nd edn., Prentice-Hall, Englewood Cliffs, NJ, 1991.
[16] D. Fan, E. White, J. Electrochem. Soc. 138 (1991) 1688.